



DIABETIC RETINOPATHY UPDATE

Magnetic resonance imaging of the retina: A brief historical and future perspective

Timothy Q. Duong *

Research Imaging Institute, Ophthalmology, Radiology, and Physiology, University of Texas Health Science Center, San Antonio, TX, USA
South Texas Veterans Health Care System, San Antonio, TX, USA

Received 11 January 2011; accepted 21 January 2011
Available online 26 January 2011

KEYWORDS

MRI;
Magnetic resonance imaging;
Diabetic retinopathy;
Retinitis pigmentosa;
Glaucoma

Abstract This invited review starts with a brief introduction of retinal anatomy and magnetic resonance imaging techniques with contrast to optics, followed by a history and future perspective on MRI applications to investigate the retinas of rodents, non-human primates and humans.

© 2011 King Saud University. Production and hosting by Elsevier B.V. All rights reserved.

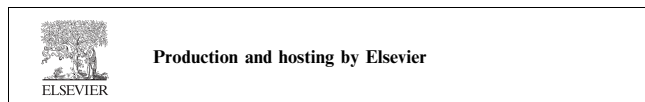
Contents

1. Introduction	138
2. Optical imaging.	138
3. Magnetic resonance imaging (MRI)	138
4. MRI of the retina	139
4.1. Rodent retina	139
4.1.1. Anatomical MRI	139
4.1.2. Blood flow MRI	140

* Address: University of Texas Health Science Center at San Antonio, Research Imaging Institute, 8403 Floyd Curl Dr, San Antonio, TX 78229, USA. Tel.: +1 567 8100; fax: +1 210 567 8152. E-mail address: duongt@uthscsa.edu

1319-4534 © 2011 King Saud University. Production and hosting by Elsevier B.V. All rights reserved.

Peer review under responsibility of King Saud University.
doi:10.1016/j.sjopt.2011.01.004



4.1.3.	fMRI of physiological challenges	140
4.1.4.	fMRI of visual stimulations	140
4.2.	Large non-human-primate retina on clinical scanner	140
4.3.	Applications to retinal diseases	140
4.4.	Human retina	140
5.	Future perspectives	141
	Acknowledgments	141
	References	141

1. Introduction

The retina consists of multiple distinct stratified layers (Wassle and Boycott, 1991). From the vitreo-retinal interface, these layers are the nerve fiber layer (NFL) + ganglion cell layer (GCL), inner plexiform layer (IPL), inner nuclear layer (INL), outer plexiform layer (OPL), outer nuclear layer (ONL), inner segment (IS), and outer segment (OS). The interspersed plexiform layers are the synaptic links between the adjacent nuclear layers. The thickness of the mammalian neural retina, excluding the *choroid*, is about 200 μm in rodents (Cheng et al., 2006; Wassle and Boycott, 1991) and 300–400 μm in humans (Bron et al., 1997; Buttery et al., 1991).

The retina is supported by two separate blood supplies, the *retinal* and *choroidal* vessels. The *retinal* vasculature is mainly localized in the ganglion cell layer, but projects capillaries into the INL, IPL, and OPL (Bill, 1984; Harris et al., 1998; Kaufman and Alm, 1992). The *choroidal* vasculature is located beneath the photoreceptor layer, between the sclera and the retinal pigment epithelium, a thin layer of epithelial cells at the base of the photoreceptor outer segment. *Choroidal* vessels do not extend into the photoreceptor layers (ONL, IS, OS) which are in fact avascular. Choroid layer thickness is sparsely reported. It has been reported to be 50 μm in rats by histology which is susceptible to fixation artifacts, 90 μm in rats in vivo (Cheng et al., 2006), and 200–300 μm in humans in vivo (Alamouti and Funk, 2003; Schuman et al., 1995; Spaide et al., 2008). The neural retina heavily relies on diffusion for oxygen delivery, primarily from the *choroidal vessels*, and transport of metabolites across the retinal pigment epithelium (Bill, 1984; Harris et al., 1998; Kaufman and Alm, 1992). The thickness of the *choroid*, which is not well documented, has been reported to be 25–45 μm in rats (Cheng et al., 2006). Importantly, the *retinal* and *choroidal* blood flows are regulated very differently. Basal *choroidal* blood flow is much higher than *retinal* blood flow, which is similar to cerebral blood flow. *Choroidal* blood flow is less responsive to many blood-flow modulating factors compared to *retinal* blood flow which responds robustly to many blood-flow modulating factors, similar to cerebral blood flow regulation (Alm and Bill, 1970; Bill, 1984; Friedman et al., 1964; Harris et al., 1998; Kaufman and Alm, 1992).

2. Optical imaging

Optical based imaging techniques have been widely utilized to study the anatomy and physiology of the retina. Methods for imaging retinal anatomy include fundus photography, optical coherence tomography (Fujimoto et al., 1995), and scanning laser ophthalmoscopy. With adaptive optics, spatial resolution can be improved so that single cone and rod cells can be visu-

alized (Zawadzki et al., 2005). Methods to image blood flow and velocity include fluorescein angiography (Preussner et al., 1983), indocyanin-green angiography (Guyer et al., 1993), laser Doppler velocimetry and flowmetry (Riva et al., 1983, 2005), and laser speckle imaging (Cheng and Duong, 2007; Cheng et al., 2008). These techniques have been used to study blood velocity and blood flow in large vessels or relative blood flow and oxygenation in tissue. Intrinsic optical imaging detecting changes in scattering and blood oxygenation has also been applied to study the retina (Grinvald et al., 2004; Hanazono et al., 2007, 2008; Tsunoda et al., 2004a,b). Optical techniques, except optical coherence tomography, are depth limited. Most optical signals come from the retinal surface with unknown extent of signal contamination from deeper layers. Optical techniques may be constrained to a small field of view and may not be used in instances where disease-induced opacity of the vitreous humor, cornea, or lens is present. Moreover, blood flow and blood velocity optical measurements are limited to large surface vessels, which may not reflect local tissue perfusion. *Choroidal* blood flow is generally inaccessible with optics because *choroid* vessels are hidden behind the retinal pigment epithelium. Nonetheless, optical imaging techniques provide important and clinically relevant information and have been widely utilized in the clinical settings.

3. Magnetic resonance imaging (MRI)

MRI provides relatively high-resolution anatomical, physiological, and functional images of the entire body non-invasively and in a single setting. MRI has no depth limitation and offers a large field of view. To date, MRI is arguably the method of choice for non-invasive anatomical imaging of many organs since it provides exquisite soft tissue contrast and structural details for clinical diagnosis. In addition, blood flow, relative blood oxygenation, and brain function can also be imaged. Anatomical, blood flow, vascular oxygenation and functional MRI techniques are briefly described below.

Anatomical contrast in MRI arise from differences in spin density, spin-lattice relaxation time (T_1), spin-spin relaxation time (T_2) and apparent diffusion coefficient of water in tissue. These MRI parameters vary depending on the properties of the local tissue environment including water content, cellular structure, macromolecule content, and ion concentrations. Many diseases alter these biophysical parameters, causing visible changes in image contrast. Moreover, alterations of these contrasts may be detectable in early stages before clinical symptoms occur, providing opportunities for early detection. In addition, the nascent capacity of anatomical MRI to distinguish different tissue types can be further enhanced by exogenous contrast agents. For example, Gd-DTPA (gadolinium-diethylene-tri-amine-pentaacetic acid), an estab-

lished, clinically approved contrast agent can be used to enhance vascular signals.

Blood flow, an important physiological parameter, can be quantitatively imaged using MRI. This can be done using an exogenous intravenous contrast agent (dynamic susceptibility contrast) or by magnetically labeling blood non-invasively to provide endogenous contrast (arterial spin-labeling (Calamante et al., 2002)). These blood-flow methods (Alsop and Detre, 1996; Detre et al., 1994; Duong et al., 2000b; Williams et al., 1992; Wong et al., 1998a,b) are widely used to measure quantitative blood flow in the brain and have been cross validated with autoradiography (Tsekos et al., 1998) and positron emission tomography (Liu et al., 2001; Zaini et al., 1999). Dynamic susceptibility contrast MRI, which requires an injection of a contrast agent, has better SNR for a single acquisition. However, it can only be performed once because of the long intravascular half-life of the contrast agent. Arterial spin labeling techniques, on the other hand, are totally non-invasive, and the labeled water has a short half-life (\sim blood T_1) making it possible to perform repeated measurements which can be used to augment spatial resolution, signal-to-noise ratio and to monitor blood flow in real time (Calamante et al., 2002).

Relative blood oxygenation can also be imaged. The technique is referred to as the blood oxygenation level dependent (BOLD) technique (Ogawa et al., 1990). BOLD MRI detects differences in MR signal intensity that arise from changes in oxygenation saturation of hemoglobin during brain activation. Deoxyhemoglobin is paramagnetic and thus introduces intravoxel magnetic field inhomogeneity which alters the MR signal, while oxyhemoglobin is diamagnetic. Susceptibility-sensitized MRI images are thus able to show changes in regional deoxyhemoglobin content. A local reduction in deoxyhemoglobin concentration will increase the BOLD signal, while an increase in deoxyhemoglobin will decrease the BOLD signal. In the brain, when a specific region is activated associated with stimulations (such as visual stimuli), local blood flow increases to compensate for the increased metabolic activity and oxygen consumption in the region. Such blood flow increases will provide a boost in oxygen delivery in excess of the increased oxygen consumption associated with increased neural activities. Local oxygen saturation, therefore, increases and deoxyhemoglobin concentration decreases. Techniques that can measure blood flow and blood oxygenation can thus be utilized to non-invasively image brain functions. These techniques are referred to as functional MRI (fMRI) techniques (Bandettini et al., 1992; Kwong et al., 1992; Ogawa et al., 1990, 1992).

Another common fMRI method is the arterial spin labeling technique which dynamically measure blood flow changes in response to stimulations. Blood-flow fMRI can be made more sensitive to blood flow in smaller vessels which better reflect local tissue perfusion and avoid contamination from large draining veins, which are prominent in typical BOLD fMRI. Moreover, blood-flow fMRI is easier to interpret because it measures a single physiological parameter, in contrast to BOLD fMRI which is affected by multiple physiological parameters, such as blood flow, blood volume, and blood oxygenation. However, blood-flow fMRI has lower temporal resolution and poorer sensitivity per unit time due to much lower signal-to-noise ratio compared to BOLD fMRI (Duong et al., 2001b). BOLD and blood-flow fMRI techniques have also been used to study

neurovascular coupling in the brain to study brain physiology and functions.

By comparison, the spatiotemporal resolution of MRI is low relative to optical imaging techniques. With rapid improvements in MRI technologies, the spatial and temporal resolutions of MRI have sufficiently advanced to allow anatomical, physiological and functional imaging of cortical layers and columnar structure in the brain (Cheng et al., 2001; Duong et al., 2000a, 2001a; Goense and Logothetis, 2006; Kim et al., 2000; Silva and Koretsky, 2002). This allows non-invasive longitudinal investigation of very small structures in vivo.

The remainder of this paper will describe a brief history and future perspective on the multimodal MRI applications to image the retinas of rodents, non-human primates and humans.

4. MRI of the retina

4.1. Rodent retina

4.1.1. Anatomical MRI

Layer-specific structural MRI has been reported in rats (Cheng et al., 2006), cats (Shen et al., 2006), and mice (Chen et al., 2008). Relaxation times and apparent diffusion coefficients have been reported in rats (Nair et al., 2010), cats (Shen et al., 2006), and mice (Chen et al., 2008). At these spatial resolutions, only three to four layers were detected. Layer thicknesses and assignments were compared with histology in these studies.

Gd-DTPA enhanced MRI can be used to enhance the retinal vessels and the choroidal vessels, bounding the retina. The retinal vessels consist of non-fenestrated capillaries which are impervious to many tracers, including Gd-DTPA, and tight-junctions between retinal epithelial cells in the choroidal circulation prevent the passage of large molecules into the neural retina, including Gd-DTPA (Vinores, 1995). Therefore, Gd-DTPA will enhance the signal in retinal and choroidal vessels, but the avascular photoreceptor layers in the retina should not show any enhancement. Gd-DTPA enhanced MRI has been reported in rat (Cheng et al., 2006) and cat (Shen et al., 2006) retinas. Gd-DTPA enhanced MRI aids in the assignment of histological layers of the retina to MRI layers.

Manganese is both an MRI contrast agent and a calcium analog. Unlike calcium, Mn is trapped in the intracellular space with a half life of few days (Cotzias et al., 1968; Newland et al., 1987), and thus selectively enhances intracellular water MRI signals. Manganese-enhanced MRI (MEMRI) has been utilized to map increased calcium-dependent neural activity and regional differences in *basal* calcium activity in the brain (Duong et al., 2000b; Lin and Koretsky, 1997) as well as to improve anatomic contrast (Aoki et al., 2004; Lee et al., 2005). Duong et al. explored the use of MEMRI to improve anatomic contrast among retinal layers (Duong et al., 2008). $MnCl_2$ was injected directly into the vitreous and imaged at $25 \times 25 \mu m$ in-plane resolution 24 h after injection. High-contrast MEMRI of normal retinas revealed seven distinct bands of alternating hyper- and hypo-intensities. The signal intensity profiles across the retinal thickness showed a diffuse bright band closest to the vitreous (#1) and three bright bands (#3, #5 and #7) interspersed among three dark bands (#2, #4, and #6). To confirm vascular layer boundaries, Gd-DTPA was injected intravenously in the same animal. Gd-DTPA enhancement

was consistently seen in retinal layers #1–#3 and in layer #7 but not in the sclera, vitreous or in retinal layers #4–#6.

4.1.2. Blood flow MRI

Li et al. was the first to report blood flow of the rat retina using MRI (Li et al., 2008). Arterial spin labeling was implemented to measure quantitative basal blood flow and blood-flow fMRI changes during physiological stimulation. Blood-flow MRI in the rat retina was performed using gradient-echo echo-planar imaging at $90 \times 90 \times 1000 \mu\text{m}$. Muir et al. markedly improved spatial resolution to visualize the retinal and choroid blood flow (Muir and Duong, 2010, in press) using a novel blood flow MRI method (Muir et al., 2008).

4.1.3. fMRI of physiological challenges

Cheng et al. investigated a layer-specific neurovascular coupling in the retina using BOLD fMRI in rats in response to physiological stimuli (Cheng et al., 2006). High resolution BOLD fMRI was obtained during hyperoxic (100% O₂) and hypercapnic (5% CO₂ + 21% O₂) challenges with air as the baseline (Cheng et al., 2006). Data were acquired with spin-echo echo-planar imaging at $90 \times 90 \times 1000 \mu\text{m}$ with diffusion weighting to suppress the overwhelmingly strong but fast-diffusing vitreous signal. Layer-specific BOLD fMRI responses were detected in two bands on the inner and outer edges of the retina. The two bands, corresponding to the retinal and choroidal vasculature, responded differently to the stimuli, indicative of differences in blood-flow regulation. Nair et al. used blood volume fMRI to image responses to hyperoxic and hypercapnic challenges with air as the baseline in the rat retinas at considerably high spatial resolution (Nair et al., 2011). This was made possible with a blood-pool contrast agent (monocrystalline iron oxide nanocolloid, MION). Their results with respect to the different responses of the retinal and choroid vascular layers are consistent with those of Cheng et al. (Cheng et al., 2006).

4.1.4. fMRI of visual stimulations

Duong et al. was the first to report BOLD fMRI responses to visual stimuli in cat retinas. BOLD fMRI of visual stimuli in rat retinas was recently reported (De La Garza et al., 2010, in press). These findings offered no laminar resolution. Shih et al. utilized MION contrast agent and resolved retinal and choroidal responses in the retinas (Shih et al., 2010, in press). They also investigated changing luminances, wavelengths (colors) and flicker frequencies. Retinal vessels were very responsive to visual stimuli and exhibited characteristic tuning curves, whereas choroidal vessels showed small percent changes and did not exhibit characteristic tuning curves.

4.2. Large non-human-primate retina on clinical scanner

Translation of retinal MRI applications from rodents to humans is faced with two major challenges: (i) hardware that limits spatial resolution and signal-to-noise ratio on clinical MRI scanners, and (ii) eye movements in awake humans. As a first step toward translation, Zhang et al. (Zhang et al., 2010b, in press) investigated the feasibility of multimodal retinal MRI on anesthetized/paralyzed large non-human primate (baboon) using a standard clinical 3-Tesla MRI scanner. Baboon was

chosen because the retina of baboon, compared to rodent, is evolutionarily closer to that of human, likely better recapitulates many human retinal diseases. The size of the baboon eye and the thickness of baboon retina are more similar to those of humans compared to rodents. Baboons have fovea in contrast to rodents and cats. Anesthesia and paralysis were used to exclude movement artifacts, such that we could focus on evaluating hardware feasibility, pulse sequence protocols and parameters for high-resolution multimodal MRI of the retinas on a clinical scanner. These multimodal MRI protocols included anatomical MRI, basal blood flow MRI, BOLD fMRI of hyperoxic challenge and blood flow fMRI of hypercapnic challenge (Zhang et al., 2010b, in press). This study presents a novel approach to visualize anatomical, physiological (BOLD and blood flow) and functional MRI of large non-human-primate retinas on a clinical scanner, and this serves as a first step toward translation.

4.3. Applications to retinal diseases

Multimodal MRI has also been applied to study retinal degeneration (Cheng et al., 2006; Li et al., 2009), diabetic retinopathy (Berkowitz et al., 2004), and glaucoma (Calkins et al., 2008; Chan et al., 2008) on rodent models.

4.4. Human retina

Zhang et al. (Zhang et al., 2010a, in press) demonstrated, for the first time, a novel MRI application to detect BOLD fMRI signal changes associated with oxygen and carbogen challenges in the unanesthetized human retina without depth limitation at reasonably high spatiotemporal resolution on a clinical 3 Tesla scanner. These findings indicate that clinical scanners have sufficient SNR, gradient strength, and stability to perform retinal BOLD fMRI in unanesthetized humans. This was made possible by optimizing a custom-designed eye coil, and the MRI sequence and sequence parameters so that they are free of susceptibility artifacts. Eye movement can be effectively managed with eye fixation, synchronized blinks, and post-processing image co-registration. BOLD fMRI has the potential to provide a valuable tool to study the retinal physiology and pathophysiology, including how vascular oxygenation is regulated at the tissue level in the normal retina in vivo, and how retinal diseases may affect oxygen response in the retina. This study provides encouraging data to further explore BOLD fMRI of the retina in unanesthetized humans. Additional improvement in spatial resolution and sensitivity is expected.

Peng et al. (Peng et al., 2010, in press) demonstrated a proof of concept that *quantitative* basal blood flow and its responses to hypercapnic challenge in unanesthetized human retina can be imaged using non-invasive MRI. A custom-designed eye surface coil improves SNR in the posterior retina compared to standard head volume coils, pseudo-continuous arterial spin-labeling technique improves sensitivity for blood flow measurement, and high turbo-spin echo acquisition yields images free of susceptibility artifacts. Synchronized eye blink minimizes eye movement and synchronized respiration reduces physiological fluctuation, respectively. The advantage of blood-flow MRI are: (i) non-invasive, (ii) depth-resolved and unhindered by media opacity, (iii) quantitative, allowing comparison across subjects, and (iv) sensitive, capable of detecting

changes associated with mild hypercapnic inhalation. MRI has the potential to provide a valuable tool to study how blood flow is regulated in the normal retina (i.e., neurovascular coupling), and how retinal diseases may affect basal blood flow and blood-flow regulation in vivo. Although improvement in spatial resolution is needed, this study sets the stage for further exploration of blood flow MRI of the human retina in normal and diseased states. Maliki et al. also recently reported blood flow MRI of the human retina albeit at lower spatial resolution (Maleki et al., 2010, in press).

5. Future perspectives

This review summarizes a brief history of development and application of lamina-specific anatomical, physiological and functional MRI to study the normal and diseased retinas. MRI reveals multiple anatomical layers within the retina, the *retinal* and *choroid* vascular layers, and the unique differential regulations of hemodynamics of the two vascular layers. The key advantages of MRI are it is non-invasive, has depth resolution and it offers multimodal (structural, physiological and functional) information. The key disadvantages of MRI are it has higher cost and lower spatiotemporal resolution which makes it more susceptible to eye movement in awake subjects relative to optical imaging techniques to date. MRI application to the retina is still in its infancy. It has many potential applications in animal models of retinal diseases. It has been translated to human applications. However, its clinical efficacy remain to be demonstrated.

There are many remaining challenges, and along comes with exciting opportunities for new development and discovery. The key challenges include: (1) improvement of spatiotemporal resolution and sensitivity, which includes developing and optimizing new arrayed detectors, pulse sequences as well as high-field scanners, (2) minimization of eye movements with cue blinks and fixations, and (3) improvement of image co-registration algorithms to improve alignment. With rapid advances in MRI technologies, we anticipate that there will be substantial improvement in the near future and MRI applications in the retina will broaden. Given the lack of competing depth-resolved, physiological imaging techniques and the challenges in obtaining quantitative blood flow (and other physiological) data in the in vivo retinas, MRI approaches to image retinal physiology and function warrant further investigations.

Acknowledgments

The author thanks his former and current team members (Qiang Shen, Haiying Cheng, Yingxia Li, Govind Nair, Eric Muir, YenYu Shih, Bryan de la Garza, Hsiao-Ying Wey, and Oscar San Emeterio Nateras), and former and current collaborators (Ross Shonat, Mabelle Pardue, Peter Thule, Darin Olson, Chris Peng, Jeffrey Kiel, Joseph Harrison, Steven Chalfin, and Carlos Rosende) for their contributions to the works reviewed in this paper.

Work on cat retina is supported by the Whitaker Foundation (RG-02-0005) and National Institute of Health/National Eye Institute (R01 EY014211). Work on rat retina is supported by the National Institute of Health/National Eye Institute (R01 EY014211 and R01 EY018855) and MERIT Award from

the Department of Veterans Affairs. Work on baboon retina is supported by the American Heart Association via the Established Investigator Award (EIA 0940104 N). Work on human retina is supported by a Pilot and Translational Technology Resource grants (parent grant UL1RR025767). Please visit <http://ric.uthscsa.edu/duong/index.htm> for more information on these projects.

References

- Alamouti, B., Funk, J., 2003. Retinal thickness decreases with age: an OCT study. *Br. J. Ophthalmol.* 87, 899–901.
- Alm, A., Bill, A., 1970. Blood flow and oxygen extraction in the cat uvea at normal and high intraocular pressures. *Acta Physiol. Scand.* 80, 19–28.
- Alsop, D., Detre, J., 1996. Reduced transit-time sensitivity in noninvasive magnetic resonance imaging of human cerebral blood flow. *J. Cereb. Blood Flow Metab.* 16, 1236–1249.
- Aoki, I., Wu, Y.J., Silva, A.C., Lynch, R.M., Koretsky, A.P., 2004. In vivo detection of neuroarchitecture in the rodent brain using manganese-enhanced MRI. *NeuroImage* 22, 1046–1059.
- Bandettini, P.A., Wong, E.C., Hinks, R.S., Rikofsky, R.S., Hyde, J.S., 1992. Time course EPI of human brain function during task activation. *Magn. Reson. Med.* 25, 390–397.
- Berkowitz, B.A., Roberts, R., Luan, H., Peysakhov, J., Mao, X., Thomas, K.A., 2004. Dynamic contrast-enhanced MRI measurements of passive permeability through blood retinal barrier in diabetic rats. *Invest. Ophthalmol. Vis. Sci.* 45, 2391–2398.
- Bill, A., 1984. Circulation in the eye. In: Renkin, E.M., Michel, C.C. (Eds.), *Handbook of Physiology Part 2 in Microcirculation*. American Physiological Society, Bethesda, MD, pp. 1001–1035.
- Bron, A.J., Tripathi, R.C., Tripathi, B.J., 1997. *Wolff's Anatomy of the Eye and Orbit*. Chapman & Hall Medical, London.
- Buttery, R.G., Hinrichsen, C.F.L., Weller, W.L., JR, H., 1991. How thick should a retina be? A comparative study of mammalian species with and without intraretinal vasculature. *Vision Res.* 31, 169–187.
- Calamante, F., Gadian, D.G., Connelly, A., 2002. Quantification of perfusion using bolus tracking magnetic resonance imaging in stroke: assumptions, limitations, and potential implications for clinical use. *Stroke* 33, 1146–1151.
- Calkins, D.J., Horner, P.J., Roberts, R., Gadianu, M., Berkowitz, B.A., 2008. Manganese-enhanced MRI of the DBA/2J mouse model of hereditary glaucoma. *Invest. Ophthalmol. Vis. Sci.* 49, 5083–5088.
- Chan, K.C., Fu, Q.L., Hui, E.S., So, K.F., Wu, E.X., 2008. Evaluation of the retina and optic nerve in a rat model of chronic glaucoma using in vivo manganese-enhanced magnetic resonance imaging. *Neuroimage* 40, 1166–1174.
- Chen, J., Wang, Q., Zhang, H., Yang, X., Wang, J., Berkowitz, B.A., Wickline, S.A., Song, S.K., 2008. In vivo quantification of T(1), T(2), and apparent diffusion coefficient in the mouse retina at 1174T. *Magn. Reson. Med.* 59, 731–738.
- Cheng, H., Nair, G., Walker, T.A., Kim, M.K., Pardue, M.T., Thule, P.M., Olson, D.E., Duong, T.Q., 2006. Structural and functional MRI reveals multiple retinal layers. *Proc. Natl. Acad. Sci. USA* 103, 17525–17530.
- Cheng, H., Duong, T.Q., 2007. Simplified laser-speckle-imaging analysis method and its application to retinal blood flow imaging. *Opt. Lett.* 32, 2188–2190.
- Cheng, H., Yan, Y., Duong, T.Q., 2008. Temporal statistical analysis of laser speckle image and its application to retinal blood-flow imaging. *Optics Express* 16, 10214–10219.
- Cheng, K., Waggoner, R.A., Tanaka, K., 2001. Human ocular dominance columns as revealed by high-field functional magnetic resonance imaging. *Neuron* 32, 359–397.

- Cotzias, G., Horiuchi, M., Fuenzalida, S., Mena, I., 1968. Clearance of tissue manganese concentrations with persistence of the neurological picture. *Neurology* 18, 376–382.
- De La Garza, B., Li, G., Muir, E., Shih, Y.Y., Duong, T.Q., 2010. BOLD fMRI of visual stimulation in the rat retina at 11.7 tesla. *NMR Biomed.*, in Press
- Detre, J.A., Zhang, W., Roberts, D.A., Silva, A.C., Williams, D.S., Grandis, D.J., Koretsky, A.P., Leigh, J.S., 1994. Tissue specific perfusion imaging using arterial spin labeling. *NMR Biomed.* 7, 75–82.
- Duong, T.Q., Kim, D.-S., Ugurbil, K., Kim, S.-G., 2000a. Spatio-temporal dynamics of the BOLD fMRI signals in cat visual cortex: toward mapping columnar structures using the early negative response. *Magn. Reson. Med.* 44, 231–242.
- Duong, T.Q., Silva, A.C., Lee, S.-P., Kim, S.-G., 2000b. Functional MRI of calcium-dependent synaptic activity: cross correlation with CBF and BOLD measurements. *Magn. Reson. Med.* 43, 383–392.
- Duong, T.Q., Kim, D.-S., Ugurbil, K., Kim, S.-G., 2001a. Localized blood flow response at sub-millimeter columnar resolution. *Proc. Natl. Acad. Sci. USA* 98, 10904–10909.
- Duong, T.Q., Kim, D.S., Ugurbil, K., Kim, S.G., 2001b. Localized cerebral blood flow response at submillimeter columnar resolution. *Proc. Natl. Acad. Sci. USA* 98, 10904–10909.
- Duong, T.Q., Pardue, M.T., Thule, P.M., Olson, D.E., Cheng, H., Nair, G., Li, Y., Kim, M., Zhang, X., Shen, Q., 2008. Layer-specific anatomical, physiological and functional MRI of the retina. *NMR Biomed.* 21, 978–996.
- Friedman, E., Kopald, H.H., Smith, T.R., 1964. Retinal and choroidal blood flow determined with krypton 85 in anesthetized animals. *Invest. Ophthalmol.* 3, 539–547.
- Fujimoto, J.G., Brezinski, M.E., Tearney, G.J., Boppart, S.A., Bouma, B., Hee, M.R., Southern, J.F., Swanson, E.A., 1995. Optical biopsy and imaging using optical coherence tomography. *Nat. Med.* 1, 970–972.
- Goense, J.B., Logothetis, N.K., 2006. Laminar specificity in monkey V1 using high-resolution SE-fMRI. *Magn. Reson. Imag.* 24, 381–392.
- Grinvald, A., Bonhoeffer, T., Vanzetta, I., Pollack, A., Aloni, E., Ofri, R., Nelson, D., 2004. High-resolution functional optical imaging: from the neocortex to the eye. *Ophthalmol. Clin. North Am.* 17, 53–67.
- Guyer, D.R., Yannuzzi, L.A., Slakter, J.S., Sorenson, J.A., Orlock, S., 1993. The status of indocyanine-green videoangiography. *Cur. Opin. Ophthalmol.* 4, 3–6.
- Hanazono, G., Tsunoda, K., Shinoda, K., Tsubota, K., Miyake, Y., Tanifuji, M., 2007. Intrinsic signal imaging in macaque retina reveals different types of flash-induced light reflectance changes of different origins. *Invest. Ophthalmol. Vis. Sci.* 48, 2903–2912.
- Hanazono, G., Tsunoda, K., Kazato, Y., Tsubota, K., Tanifuji, M., 2008. Evaluating neural activity of retinal ganglion cells by flash-evoked intrinsic signal imaging in macaque retina. *Invest. Ophthalmol. Vis. Sci.* 49, 4655–4663.
- Harris, A., Kagemann, L., Cioffi, G.A., 1998. Assessment of human ocular hemodynamics. *Surv. Ophthalmol.* 42, 509–533.
- Kaufman, P.L., Alm, A. (Eds.), 1992. *Adler's Physiology of the Eye*. Mosby, St Louis.
- Kim, D.-S., Duong, T.Q., Kim, S.-G., 2000. High-resolution mapping of iso-orientation columns by fMRI. *Nat. Neurosci.* 3, 164–169.
- Kwong, K., Hoppel, B., Weisskoff, R., Kihne, S., Barrere, B., Moore, J., Poncelet, B., Rosen, B., Thulborn, K., 1992. Regional cerebral tissue oxygenation studied with EPI at clinical field strengths. *J. Magn. Reson. Imag.* 2, 44.
- Lee, J.H., Silva, A.C., Merkle, H., Koretsky, A.P., 2005. Manganese-enhanced magnetic resonance imaging of mouse brain after systemic administration of MnCl₂: dose-dependent and temporal evolution of T1 contrast. *Magn. Reson. Med.* 53, 640–648.
- Li, Y., Cheng, H., Duong, T.Q., 2008. Blood-flow magnetic resonance imaging of the retina. *Neuroimage* 39, 1744–1751.
- Li, Y., Cheng, H., Shen, Q., Kim, M., Thule, P.M., Olson, D.E., Pardue, M.T., Duong, T.Q., 2009. Blood-flow magnetic resonance imaging of retinal degeneration. *Invest. Ophthalmol. Vis. Sci.* 50, 1824–1830.
- Lin, Y.-J., Koretsky, A.P., 1997. Manganese ion enhances T1-weighted MRI during brain activation: an approach to direct imaging of brain function. *Magn. Reson. Med.* 38, 378–398.
- Liu, H.L., Kochunov, P., Hou, J., Pu, Y., Mahankali, S., Feng, C.M., Yee, S.H., Wan, Y.L., Fox, P.T., Gao, J.H., 2001. Perfusion-weighted imaging of interictal hypoperfusion in temporal lobe epilepsy using FAIR-HASTE: comparison with H₂(15)O PET measurements. *Magn. Reson. Med.* 45, 431–435.
- Maleki, N., Dai, W., Alsop, D.C., 2010. Blood flow quantification of the human retina with MRI. *NMR Biomed.*, in press
- Muir, E.R., Shen, Q., Duong, T.Q., 2008. Cerebral blood flow MRI in mice using the cardiac-spin-labeling technique. *Magn. Reson. Med.* 60, 744–748.
- Muir, E.R., Duong, T.Q., 2010. MRI of retinal and choroid blood flow with laminar resolution. *NMR Biomed.*, in press (online Sept. 6, 2010).
- Nair, G., Shen, Q., Duong, T.Q., 2010. Relaxation time constants and apparent diffusion coefficients of rat retina at 7 tesla. *Int. J. Imag. Syst. Technol.* 20, 126–130.
- Nair, G., Tanaka, Y., Kim, M., Olson, D.E., Thule, P.M., Pardue, M.T., Duong, T.Q., 2011. MRI reveals differential regulation of retinal and choroidal blood volumes in rat retina. *Neuroimage* 54, 1063–1069.
- Newland, M., Cox, C., Hamada, R., Oberdoerster, G., Weiss, R., 1987. The clearance of manganese chloride in the primate. *Fundam. Appl. Toxicol.* 9, 314–328.
- Ogawa, S., Lee, T.-M., Kay, A.R., Tank, D.W., 1990. Brain magnetic resonance imaging with contrast dependent on blood oxygenation. *Proc. Natl. Acad. Sci. USA* 87, 9868–9872.
- Ogawa, S., Tank, D.W., Menon, R., Ellermann, J.M., Kim, S.-G., Merkle, H., Ugurbil, K., 1992. Intrinsic signal changes accompanying sensory stimulation: functional brain mapping with magnetic resonance imaging. *Proc. Natl. Acad. Sci. USA* 89, 5951–5955.
- Peng, Q., Zhang, Y., Oscar San Emeterio Nateras, O., van Osch, M.J.P., Duong, T.Q., 2010. Magnetic resonance imaging of blood flow of the human retina. *Magn. Reson. Med.*, in press
- Preussner, P.R., Richard, G., Darrelmann, O., Weber, J., Kreissig, I., 1983. Quantitative measurement of retinal blood flow in human beings by application of digital image-processing methods to television fluorescein angiograms. *Graefes Arch. Clin. Exp. Ophthalmol.* 221, 110–112.
- Riva, C.E., Grunwald, J.E., Sinclair, S.H., 1983. Laser Doppler velocimetry study of the effect of pure oxygen breathing on retinal blood flow. *Invest. Ophthalmol. Vis. Sci.* 24, 47–51.
- Riva, C.E., Logean, E., Falsini, B., 2005. Visually evoked hemodynamic response and assessment of neurovascular coupling in the optic nerve and retina. *Progress Retinal Eye Res.* 24, 183–215.
- Schuman, J.S., Hee, M.R., Puliafito, C.A., Wong, C., Pedut-Kloizman, T., Lin, C.P., Hertzmark, E., Izatt, J.A., Swanson, E.A., Fujimoto, J.G., 1995. Quantification of nerve fiber layer thickness in normal and glaucomatous eyes using optical coherence tomography. *Arch. Ophthalmol.* 113, 586–596.
- Shen, Q., Cheng, H., Pardue, M.T., Chang, T.F., Nair, G., Vo, V.T., Shonath, R.D., Duong, T.Q., 2006. Magnetic resonance imaging of tissue and vascular layers in the cat retina. *J. Magn. Reson. Imaging* 23, 465–472.
- Shih, Y.Y., De La Garza, B.H., Muir, E.R., Rogers, W.E., Harrison, J.M., Kiel, J.W., Duong, T.Q., 2010. Lamina-specific functional MRI of retinal and choroidal responses to visual stimuli, in press
- Silva, A.C., Koretsky, A.P., 2002. Laminar specificity of functional MRI onset times during somatosensory stimulation in rat. *Proc. Natl. Acad. Sci. USA* 99, 15182–15187.

- Spaide, R.F., Koizumi, H., Pozzoni, M.C., 2008. Enhanced depth imaging spectral-domain optical coherence tomography. *Am. J. Ophthalmol.* 146, 496–500.
- Tsekos, N.V., Zhang, F., Merkle, H., Nagayama, M., Iadecola, C., Kim, S.-G., 1998. Quantitative measurements of cerebral blood flow in rats using the FAIR technique: correlation with previous iodoantipyrine autoradiographic studies. *Magn. Reson. Med.* 39, 564–573.
- Tsunoda, K., Oguchi, Y., Hanazona, G., Tanifuji, M., 2004a. Mapping cone- and rod-induced retinal responsiveness in macaque retina by optical imaging. *Invest. Ophthalmol. Vis. Sci.* 45, 3820–3826.
- Tsunoda, K., Oguchi, Y., Hanazono, G., Tanifuji, M., 2004b. Mapping cone- and rod-induced retinal responsiveness in macaque retina by optical imaging. *Invest. Ophthalmol. Vis. Sci.* 45, 3820–3826.
- Vinores, S.A., 1995. Assessment of blood-retinal barrier integrity. *Histol. Histopathol.* 10, 141–154.
- Wassle, H., Boycott, B.B., 1991. Functional architecture of the mammalian retina. *Physiol. Rev.* 1, 447–480.
- Williams, D.S., Detre, J.A., Leigh, J.S., Koretsky, A.P., 1992. Magnetic resonance imaging of perfusion using spin inversion of arterial water. *Proc. Natl. Acad. Sci. USA* 89, 212–216.
- Wong, E.C., Buxton, R.B., Frank, L.R., 1998a. A theoretical and experimental comparison of continuous and pulsed arterial spin labeling techniques for quantitative perfusion imaging. *Magn. Reson. Med.* 40, 348–355.
- Wong, E.C., Buxton, R.B., Frank, L.R., 1998b. Quantitative imaging of perfusion using a single subtraction (QUIPSS and QUIPSSII). *Magn. Reson. Med.* 39, 702–708.
- Zaini, M.R., Strother, S.C., Andersen, J.R., Liow, J.-S., Kjems, U., Tegeler, C., Kim, S.-G., 1999. Matching spatial resolution of coregistered PET and 4.0T fMRI brain volumes. *Med. Phys.* 26, 1559–1567.
- Zawadzki, R.J., Jones, S.M., Olivier, S.S., Zhao, M., Bower, B.A., Izatt, J.A., Choi, S., Laut, S., Werner, J.S., 2005. Adaptive-optics optical coherence tomography for high-resolution and high-speed 3D retinal in vivo imaging. *Optics Exp.* 13, 8532–8546.
- Zhang, Y., Peng, Q., Kiel, J.W., Rosende, C.A., Duong, T.Q., 2010a. Magnetic resonance imaging of vascular oxygenation changes during hyperoxia and carbogen challenges in the human retina. *Invest. Ophthalmol. Vis. Sci.*, in press, (online Sept 16 2010).
- Zhang, Y., Wey, H.Y., Oscar San Emeterio Nateras, O., Peng, Q., De La Garza, B.H., Duong, T.Q., 2010b. Anatomical, BOLD, blood-flow MRI of non-human primate (baboon) retina, in press.